Role of s−p Orbital Mixing in the Bonding and Properties of Second-Period Diatomic Molecules

F. Matthias Bickelhaupt,*,† Jeffrey K. Nagle,*,‡ and William L. Klemm‡,§

Contribution from the Scheikundig Laboratorium der Vrije Universiteit, De Boelelaan 1083, NL-1081 HV Amsterdam, The Netherlands and the Department of Chemistry, Bowdoin College, 6600 College Station, Brunswick, Maine 04011-8466

Received: October 25, 2007; In Final Form: December 17, 2007

Qualitative molecular orbital theory is widely used as a conceptual tool to understand chemical bonding. Symmetry-allowed orbital mixing between atomic or fragment orbitals of different energies can greatly complicate such qualitative interpretations of chemical bonding. We use high-level Amsterdam Density Functional calculations to examine the issue of whether orbital mixing for some familiar second-row homonuclear and heteronuclear diatomic molecules results in net bonding or antibonding character for a given molecular orbital. Our results support the use of slopes of molecular orbital energy versus bond distance plots (designated radial orbital-energy slope: ROS) as the most useful criterion for making this determination. Calculated atomic charges and frontier orbital properties of these molecules allow their acid−base chemistry, including their reactivities as ligands in coordination chemistry, to be better understood within the context of the Klopman interpretation of hard and soft acid−base theory. Such an approach can be extended to any molecular species.

1. Introduction

Molecular orbital (MO) theory is the most widely used quantum-based method for understanding chemical bonding. Even introductory chemistry textbooks routinely use it to describe the bonding in both molecules and solids.[1] Nearly all introductions to molecular orbital theory begin with its application to first- and second-period homonuclear diatomic molecules like H_2, N_2, and O_2. Scheme 1 shows the well-known generic orbital-interaction diagram for second-period homonuclear diatomics A_2. In Σ symmetry, the bonding and antibonding MOs are derived from the 2s AOs (σ_s and σ_s*; in black) and from the $2p_z$ (or $2p_\sigma$) AOs (σ_p and σ_p*; in red). Similarly, in Π symmetry, the bonding and antibonding MOs are derived from the $2p_x$ and $2p_y$ (or $2p_\pi$) AOs (π and π*; in blue).

These non-mathematical, qualitative applications of molecular orbital theory to chemical bonding present many difficulties, one of the most notable being the role of s−p orbital mixing in second-period diatomic molecules. This is illustrated below in Scheme 2 for σ-orbital interactions of a homonuclear diatomic molecule A_2. Here, the π-orbitals and their interactions are left out for clarity because their orthogonality to the 2s AOs prevents them from participating in such s−p mixing. To the left in Scheme 2, the hypothetical situation with no s−p mixing is shown: there is only mutual interaction between the 2s AOs and between the $2p_\sigma$ AOs, yielding the corresponding "first-order" bonding and antibonding combinations σ_s and σ_s*, and σ_p and σ_p*. In practice, there is always some s−p mixing. This can be conceived as arising from a "second-order" interaction between the bonding σ_s and σ_p, and between the antibonding σ_s* and σ_p* combinations, indicated by arrows on the right-hand side in Scheme 2. Consequently, the 2s-derived σ_s and σ_s* MOs receive a stabilizing admixture of σ_p and σ_p*, respectively, and vice versa, the 2p-derived σ_p and σ_p* MOs receive a *destabilizing* admixture of σ_s and σ_s*.

SCHEME 1

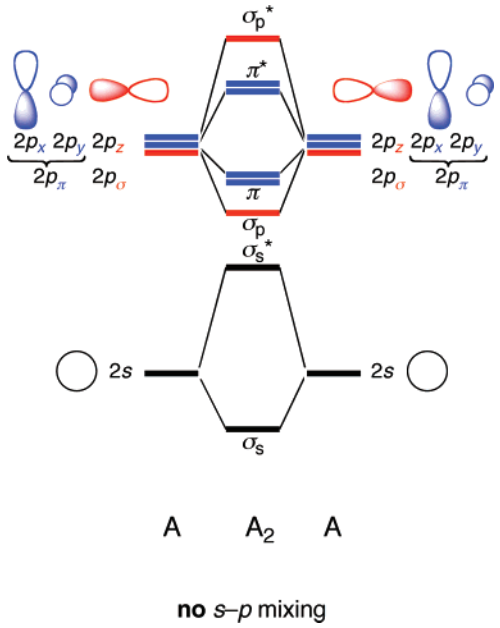

Such s−p orbital mixing in σ-orbitals is used to explain why the relative σ_p- and π-bonding molecular orbital energies are different for B_2, C_2, and N_2 compared to O_2, F_2, and Ne_2.[2] The increasing 2s−2p atomic orbital energy separation that occurs across the series B to Ne results in decreasing degrees of s−p orbital mixing, and that in turn alters the energy and bonding nature of the highest occupied σ-molecular orbital. A related and well-known additional complication occurs in the case of

† Vrije Universiteit Amsterdam.
‡ Bowdoin College.
§ Current address: Department of Physics, University of California at Berkeley.

10.1021/jp710328f CCC: $40.75
Published on Web 02/28/2008

SCHEME 2

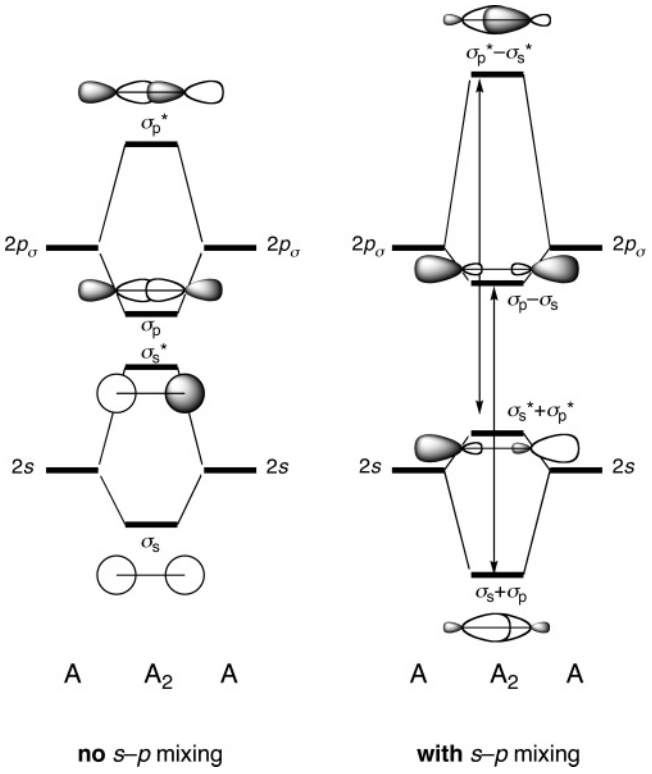

heteronuclear diatomic molecules like CO. Now the two atoms have both different 2s−2p energy separations and a mismatch in their energies such that the more electronegative atom in some cases has both lower 2s and 2p orbital energies than its less electronegative partner. The differing 2s−2p energy separations and mismatches greatly complicate the construction of qualitative molecular orbital correlation diagrams for these molecules.[3]

In this paper we use numerical results of high-level density functional (DFT) calculations[4] employing the Amsterdam Density Functional (ADF) program[5] in an effort to enhance our qualitative understanding of chemical bonding and its relationship to chemical reactivity. The accuracy of DFT calculations for small diatomic molecules has been assessed elsewhere.[6] Given the widespread use of second-period diatomic molecules as vehicles to introduce qualitative molecular orbital theory in introductory textbooks,[1−3] and the importance of these molecules as ligands in coordination and organometallic chemistry,[7] we chose them as the focus of our study. We selected the isoelectronic species N_2, CO, BF, NO^+, and CN^- to illustrate essential features of s−p orbital mixing, together with F_2, a molecule with a large 2s−2p orbital energy separation and hence relatively little s−p orbital mixing. Our analysis of the bonding in these diatomic molecules is based on the quantitative molecular orbital (MO) model contained in Kohn−Sham density functional theory (KS-DFT), which allows for a transparent description not only of the main trends but also of the more subtle yet essential features of the bonding mechanism.[5]

We focus in particular on the nature of the highest occupied σ-molecular orbital of our model diatomic molecules (5σ in all cases), which plays a key role in their function as ligands in coordination compounds.[7] Thus, we report differences in calculated equilibrium bond distances and stretching frequencies between our model diatomic molecules (*i.e.*, N_2, CO, BF, NO^+, CN^-, and F_2) and their 5σ one-electron oxidized counterparts. These differences are interpreted in terms of the energy slopes of the HOMO as a function of internuclear distance (designated radial orbital-energy slope: ROS), and we evaluate the use of such slopes as a measure of the net bonding or antibonding character of molecular orbitals in general.[8] Furthermore, the meaning and usefulness of atomic charges for atoms in these molecules is examined by comparing several different ways of calculating them.[9]

Our work complements recently reported studies that focus on an energy partition analysis of several neutral diatomic molecules, including N_2, CO, BF, and F_2.[10] The authors of those studies also employed ADF calculations as the basis for their analysis of the bonding. One of their key results was to demonstrate the dominance of σ bonding relative to π bonding in all of the molecules studied.[10a] Their interpretation of the nature of the HOMO in CO[10b] differs from the more common approach used here, and we explore this difference in some detail below.

2. Theoretical Methods

All calculations were performed with the Amsterdam Density Functional (ADF) program.[11] The numerical integration was performed using the procedure developed by Boerrigter, te Velde, and Baerends (with integration accuracy ACCINT = 10; for the VDD analysis: ACCINT = 12 and DISHUL = 20).[11d,e] The MOs were expanded in a large, uncontracted set of Slater type orbitals (STOs) containing diffuse functions, which is of triple-ζ quality for all atoms and is augmented with two sets of polarization functions: 3d and 4f on B, C, N, O, and F; and 2p and 3d on H (designated TZ2P in ADF-2007).[11f] All electrons were included in the variational treatment (*i.e.*, no frozen-core approximation was applied). An auxiliary set of s, p, d, f, and g STOs was used to fit the molecular density and to represent the Coulomb and exchange-correlation potentials accurately in each self-consistent field (SCF) cycle (with SCF convergence criterion CONVERGE = 10^{-10}).[11g]

Energies, geometries (with geometry convergence criterion CONVERGE = 10^{-8}), vibrational frequencies and the orbital electronic structure were calculated using the generalized gradient approximation (GGA) of density functional theory (DFT) at the BP86 level. The GGA proceeds from the local density approximation (LDA), where exchange is described by Slater's $X\alpha$ potential[11h] and correlation is treated in the Vosko−Wilk−Nusair (VWN) parametrization,[11i] and is augmented with nonlocal corrections to exchange due to Becke[11j,k] and correlation due to Perdew[11l] added self-consistently.[11m] Relativistic effects were taken into account in all cases using the zeroth-order relativistic approximation (ZORA).[12] Radial orbital-energy slope (ROS) values were calculated from 3-point linear transit calculations in which orbital energies at the equilibrium bond distance together with distances longer and shorter by 0.01 Å were found to vary in a very nearly linear fashion.

The orbital electronic structure and bonding in the various diatomics were analyzed in terms of the quantitative molecular orbital (MO) model contained in Kohn−Sham DFT.[5a,13]

The electron density distribution was analyzed using the Voronoi deformation density (VDD) method[9d−g] and the Hirshfeld scheme[14] for computing atomic charges. The VDD atomic charge Q_A^{VDD} was computed as the (numerical) integral[11d,e] of the deformation density $\Delta\rho(\mathbf{r}) = \rho(\mathbf{r}) - \sum_B \rho_B(\mathbf{r})$ in the volume of the Voronoi cell of atom A (eq 1).

$$Q_A^{VDD} = -\int_{\substack{\text{Voronoi}\\ \text{cell of A}}} (\rho(\mathbf{r}) - \sum\nolimits_B \rho_B(\mathbf{r}))\, d\mathbf{r} \qquad (1)$$

Here, $\rho(\mathbf{r})$ is the electron density of the molecule and $\sum_B \rho_B(\mathbf{r})$ the superposition of atomic densities ρ_B of a promolecule, a fictitious species lacking chemical interactions and corresponding to the situation in which all atoms are neutral. The Voronoi cell of atom A is defined as the compartment of space bounded by the bond midplanes on and perpendicular to all bond axes between nucleus A and its neighboring nuclei (cf. the Wigner−Seitz cells in crystals[9g]).

The interpretation of the VDD charge Q_A^{VDD} is rather straightforward and transparent. Instead of measuring the amount of charge associated with a particular atom A, Q_A^{VDD} directly monitors how much charge flows, due to chemical interactions, out of ($Q_A^{VDD} > 0$) or into ($Q_A^{VDD} < 0$), the Voronoi cell of atom A, that is, the region of space that is closer to nucleus A than to any other nucleus.

3. Results and Discussion

General Features of σ-Bonding in the Molecules. We restrict our consideration of the bonding in these second period diatomic molecules to σ interactions only because π interactions for these species do not involve the complication of s−p orbital mixing. The ADF calculated bond distances, orbital energies, and stretching frequencies for these molecules are all in excellent agreement with available experimental values.[15] Figure 1 (top) shows molecular orbital correlation diagrams based on ADF calculations for F_2, N_2, CO, and BF at the calculated internuclear equilibrium distance for each molecule (MO diagrams for N_2, CO, and BF that include both σ and π interactions are provided in the Supporting Information). Although F_2 is not isoelectronic with the other molecules, it is included here as an example of a species that does not experience significant $2s-2p_\sigma$ orbital mixing. This is confirmed for F_2 by the small Mulliken 2s orbital percentage contributions to the 5σ and 6σ MOs and the small $2p_\sigma$ orbital percentages for the 3σ and 4σ MOs (note that we use $C_{\infty v}$ symmetry labels, *i.e.*, without g or u subscripts, for designating all diatomic MOs to enable a more straightforward comparison between MOs of homonuclear and heteronuclear molecules). The small $2s-2p_\sigma$ orbital mixing is largely a result of the large calculated energy difference of 16 eV between these orbitals because, as shown in Table 1 (middle), the overlap integrals for the $2s-2p_\sigma$ interactions of F_2 are actually somewhat larger than the corresponding 2s−2s and $2p_\sigma-2p_\sigma$ values (Scheme 2, left side). The smaller 2s−2p orbital energy difference for N_2 together with the larger $2s-2p_\sigma$ spatial overlaps both contribute to the extensive $2s-2p_\sigma$ orbital mixing that raises the energy of the 5σ well above the value it would have in the absence of such mixing (Scheme 2, right side). In fact, as is well-known and often stated in introductory textbooks,[1−3] the 5σ MO becomes the HOMO in N_2, lying higher in energy than the filled and degenerate 1π MOs.

For CO and BF the smaller 2s−2p orbital energy differences for C and B compared to N result in even greater mixing of these orbitals. This decreased 2s−2p energy difference together with the nearly degenerate (less than 3 eV) C 2s and O $2p_\sigma$ energies for CO and the *higher* energy of the B 2s orbital relative to that of F $2p_\sigma$ in BF greatly complicate the nature of the σ bonding in these molecules.

Scheme 3 illustrates the situation for CO by showing the hypothetical limiting cases of C 2s−O $2p_\sigma$ orbital mixing only (left) and C $2p_\sigma$−O $2p_\sigma$ mixing only (center). The real situation that includes all types of σ orbital mixings is shown on the right side. As indicated, the 5σ HOMO has both bonding and antibonding contributions that lead to an approximately overall nonbonding character for this orbital.

Criteria for Determination of Bonding versus Antibonding Orbital Character. Although the 5σ HOMO in CO is approximately nonbonding, it is generally regarded to be slightly antibonding in nature.[7b,16] The experimental evidence cited to support this assertion is that loss of one electron from this orbital to give CO^+ leads to a contraction of the C−O bond distance and an increase in the C−O stretching force constant.[15a] Frenking, et al., have recently challenged this interpretation on the basis of ADF calculations.[10b] They claim that the lack of a node in the internuclear region between C and O for the 5σ orbital is not consistent with antibonding character for this orbital. Although this interpretation may be correct for strongly antibonding orbitals, it does not necessarily apply to weakly antibonding orbitals such as this. A quantitative criterion for evaluating the bonding character of a molecular orbital is preferable to such a visual inspection of orbital contour plots.

Fortunately, such a quantitative basis for establishing whether a molecular orbital is bonding or antibonding has been available since the earliest days of molecular orbital theory.[8] This criterion is the slope of the energy of a molecular orbital as a function of increasing distance between bonded atoms in a molecule that we designate as Radial Orbital-Energy Slope (ROS). Very simply, a positive ROS corresponds to bonding character and a negative ROS to antibonding character.[8] This criterion is perhaps not as widely known and appreciated as it should be, particularly now that its validity has been confirmed in a detailed study that focused on the photoelectron spectra of small molecules and their interpretation via restricted Hartree−Fock calculations.[8d] Walsh diagrams illustrate the variation of MO energies with change in the angular geometry of a molecule and complement the radial approach to bond energy changes considered here. A detailed evaluation of both radial and angular orbital energy variations, for both diatomic and polyatomic molecules, has been considered elsewhere.[8d]

As shown in Table 1 (top), the 5σ HOMO of CO has a small negative ROS at the calculated equilibrium distance for CO, consistent with the widely held view of this orbital as slightly antibonding in character. In contrast to CO, N_2 experiences a slight elongation and force constant decrease upon loss of an electron from its 5σ HOMO to form N_2^+. This is consistent with the small, positive ROS for this orbital, indicative of its weakly bonding character. As pointed out earlier[7b,10b] the small, negative value of the Mulliken overlap population for the 5σ orbital of N_2 misleadingly suggests weakly antibonding character for this orbital. This supports the superiority of the ROS criterion over Mulliken overlap populations for determining the bonding character of an orbital.

Inspection of the ROS values in Figures 1 and 2 and Table 1 for all six diatomic molecules reassuringly shows large, positive values for the strongly bonding 3σ orbitals and negative values for all of the strongly antibonding 6σ orbitals. Interestingly the ROS values of the 4σ orbitals for most of the molecules are substantially negative, consistent with a moderate-to-strong antibonding nature for these orbitals. The exceptions are CO and BF, which have a small, negative ROS and a large positive ROS for this orbital, respectively, indicating that the 4σ orbital is weakly antibonding in CO and significantly bonding in BF. These observations can be understood with reference to the MO correlation diagrams for these species (Figure 1, top), which show decreasing participation of the 2s orbital from the more electronegative atom in the 4σ MO as its energy drops significantly below the 2s orbital energy of the less electronegative atom. To put it another way, the B 2s overlap with F $2p_\sigma$ is largely responsible for the bonding nature of the 4σ orbital

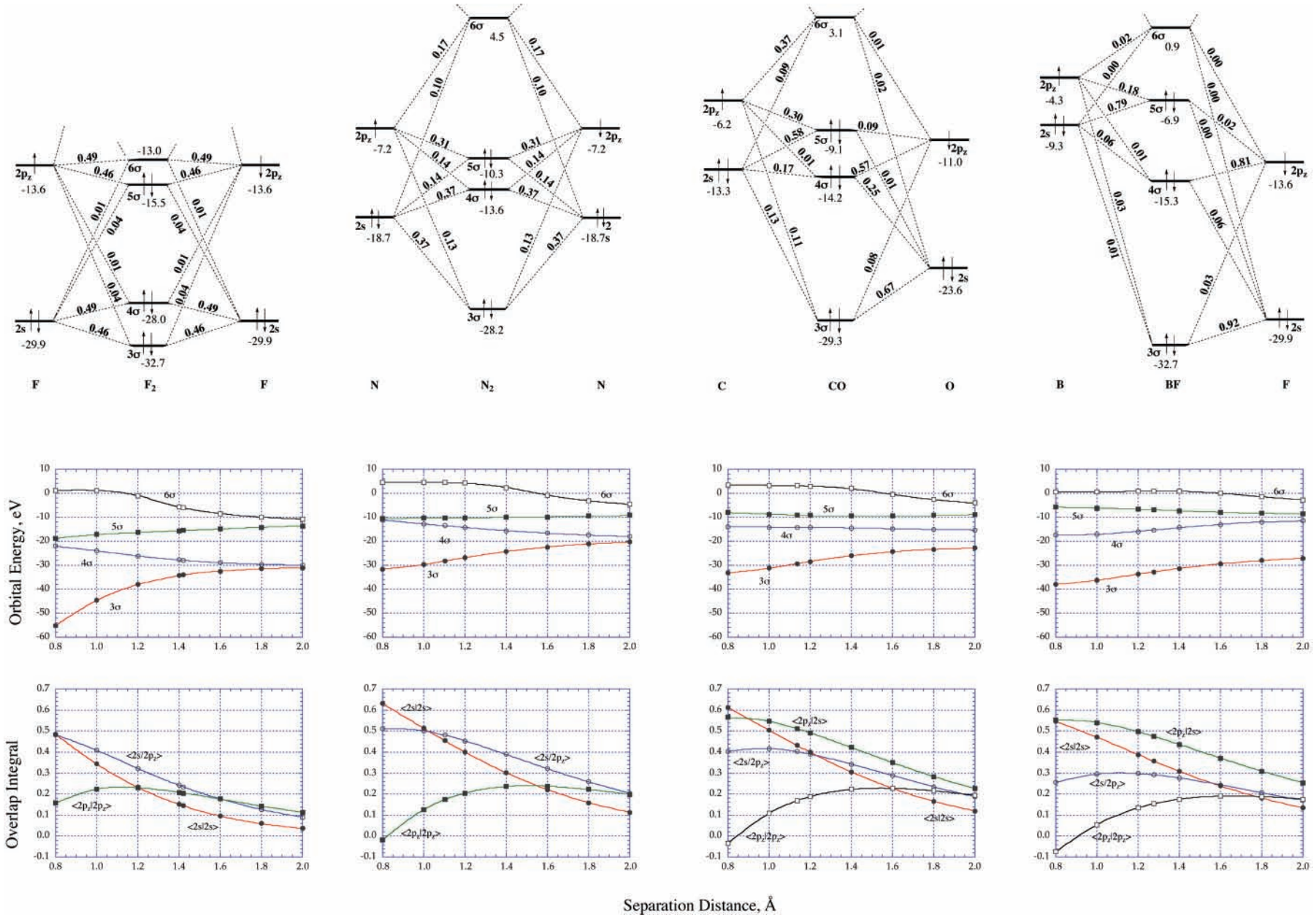

Figure 1. Molecular orbital correlation diagrams (top), molecular orbital energy variations as a function of atom separation distance (middle), and atomic orbital overlap integral variations as a function of atom separation for F_2, N_2, CO, and NO^+ (bottom). The MO correlation diagrams correspond to calculated equilibrium bond distances, with the calculated orbital energy listed below each orbital and the Mulliken AO contribution to each MO listed above each dashed connector line.

TABLE 1: ADF-Calculated Orbital Energy Slopes, Orbital Energy Overlap Integrals, And Atomic Charges

	F_2	N_2	CO	BF	NO^+	CN^-
	Bond Indicator: Radial Orbital Energy Slope (ROS; eV/Å) at Calculated Equilibrium Distance[a]					
3σ	12.2	14.5	14.2	12.1	24.5	7.6
4σ	−6.7	−7.4	−0.6	7.4	−3.4	−5.6
5σ	3.9	0.6	−2.4	−3.1	1.5	−1.6
6σ	−16.6	−1.8	−1.9	−2.1	−6.7	−1.8
	σ-Orbital Overlap Integral $\langle A\|B\rangle$ at Calculated Equilibrium Distance[a]					
$\langle 2s\|2s\rangle$	0.14	0.45	0.43	0.36	0.42	0.46
$\langle 2s\|2p_z\rangle$	0.23	0.48	0.40	0.29	0.44	0.51
$\langle 2p_z\|2s\rangle$	0.23	0.48	0.51	0.47	0.48	0.45
$\langle 2p_z\|2p_z\rangle$	0.21	0.17	0.17	0.15	0.19	0.16
	VDD (Hirshfield) Charge Q/e on Atom A					
0.8 Å	0	0	−0.05 (0.05)	−0.17 (0.01)	0.51 (0.54)	−0.53 (−0.48)
equil	0	0	0.08 (0.08)	0.06 (0.06)	0.56 (0.57)	−0.48 (−0.49)
2.0 Å	0	0	0.26 (0.23)	0.37 (0.34)	0.65 (0.64)	−0.40 (−0.44)

[a] The ADF-calculated equilibrium bond distances: F_2, 1.415 Å; N_2, 1.102 Å; CO, 1.135 Å; BF, 1.273 Å; NO^+, 1.070 Å; CN^-, 1.181 Å. These values are all longer by 0.007−0.010 Å than the corresponding experimental values with the exception of F_2, whose calculated value is 0.020 Å longer than the experimental one.

SCHEME 3

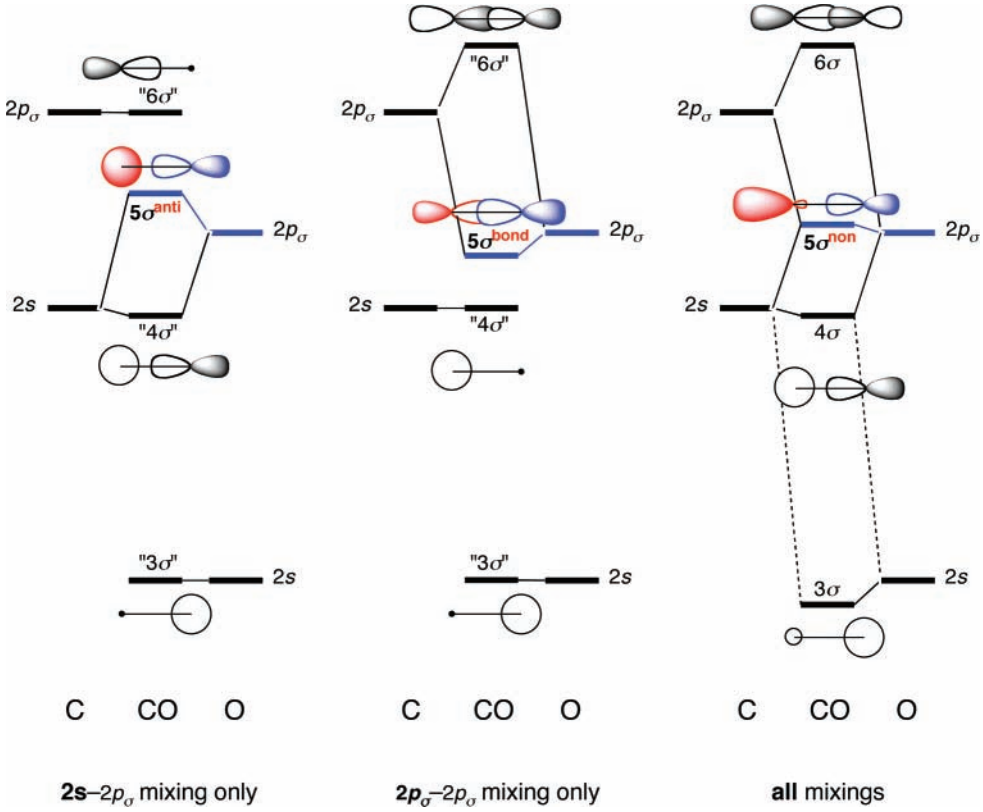

in BF, similar (but not identical) to the situation shown in the left panel of Scheme 3 for CO.

As shown in Figure 2, BF has a slightly more negative, and CN^- a slightly less negative, 5σ ROS than CO. This indicates a somewhat stronger antibonding character for this orbital in BF relative to CO, and just the opposite in CN^-. The other three diatomic molecules included in Table 1 all have positive ROS values for this orbital, indicating the 5σ orbital to be somewhat bonding in these cases.

It is tempting to explore whether there is a quantitative relationship between the magnitude of the 5σ ROS values and the bond distance and stretching force constant changes that occur upon removal of one electron from this orbital in these diatomic molecules to give their one electron ionized counterparts. Figure 3 shows plots of the calculated values of changes in the bond distance (Δd) and stretching force constant (Δk) as a function of the 5σ ROS values. Gratifyingly, in all cases Δd contractions correspond to negative ROS values, and elongations to positive ROS values. Similarly, in all cases stretching force constant increases correspond to negative ROS values, and decreases to positive ROS values. Moreover, with the exception of CO, increasing ROS values correspond to decreasing Δk values and increasing Δd values.

The sensitivity of the calculated ROS values to the exchange and correlation functional used was investigated by calculating 4σ and 5σ ROS values for CO (TZ2P basis sets in all cases) with the LDA and ten different GGA potentials. The ROS values for 4σ varied by no more than 0.17 eV/Å, and those for 5σ varied by no more than 0.06 eV/Å from the BP86 values reported in Table 1. There was a greater sensitivity to the basis set used in the calculations. Although calculations for TZP, TZ2P, and QZ4P basis sets (BP86 GGA in all cases) yielded

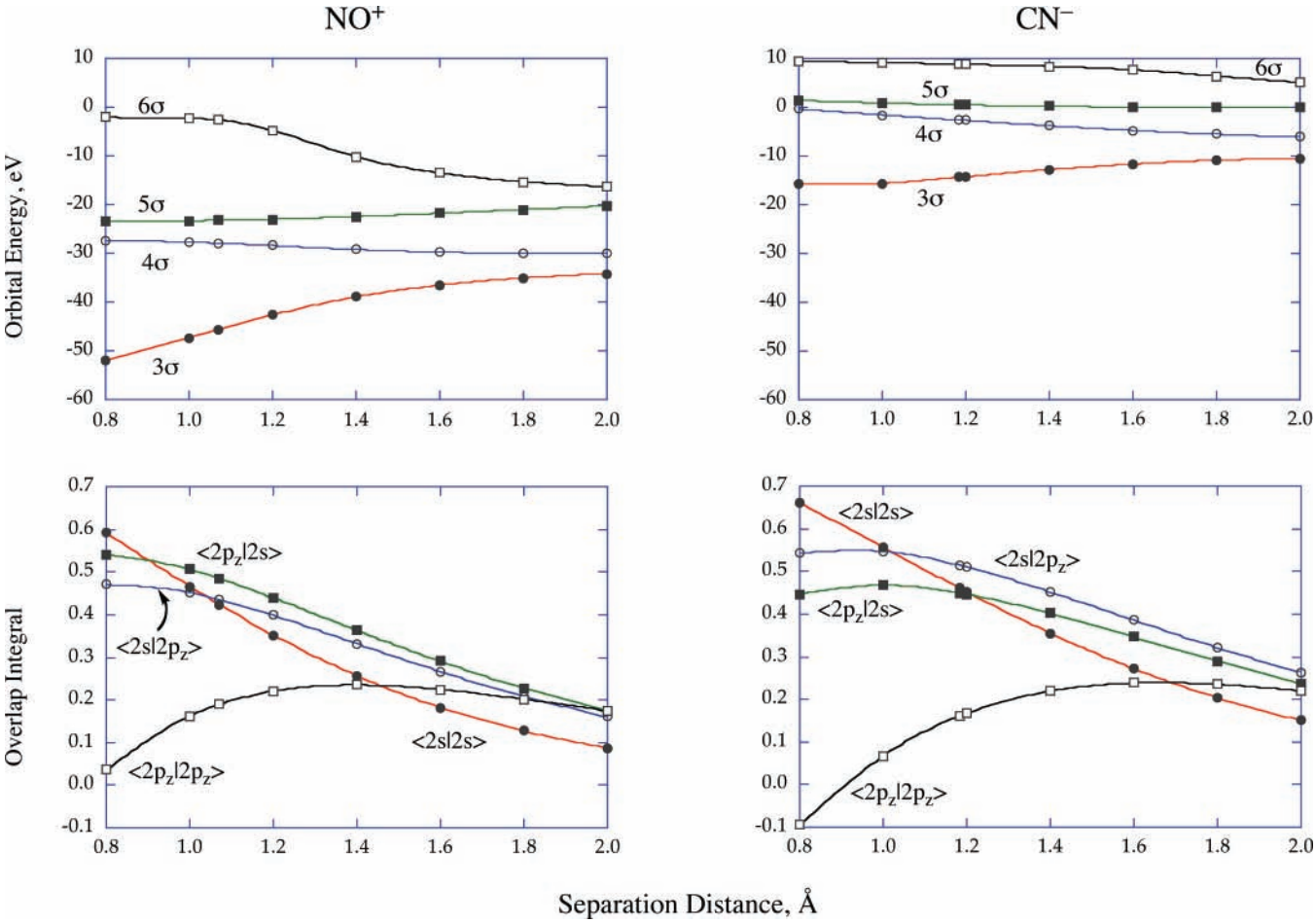

Figure 2. Orbital energies (top) and overlap integrals as a function of atom separation for NO^+ and CN^- (bottom).

4σ and 5σ ROS values for CO within a range of 0.12 and 0.11 eV/Å, respectively, lower level basis set calculations showed much greater variations.[17] To obtain reliable quantitative ROS values, it appears that basis sets of at least TZP quality should be used together with the LDA or any GGA functional. Note that, unlike Mulliken overlap populations, the ROS values *converge* as a function of basis-set size.

In addition to the molecules studied here in more detail, ADF calculations on Li_2, which has a 3σ bonding HOMO with a positive ROS (+0.24 eV/Å), reveal it to undergo the expected bond lengthening and decrease in stretching force constant upon ionization to Li_2^+. In contrast, ADF calculations on Be_2, which has a 4σ antibonding HOMO with a negative ROS (−0.22 eV/Å), show a bond shortening and increase in stretching force constant upon ionization to Be_2^+. In fact the numerical values of the stretching force constant changes for Li_2 and Be_2 (−0.16 N/cm and +0.025 N/cm, respectively) fit nicely with the values plotted for the other diatomic molecules in Figure 3. However, as for F_2, the numerical values of Δd for Li_2 and Be_2 (+0.37 and −0.22 Å, respectively) do not fit well with the other five diatomic species, all of which possess a triple bond in the most common Lewis structure used to represent their bonding. In any case it is reassuring that for all the diatomic molecules considered here, including F_2, Li_2, and Be_2, the calculated and experimental *signs* of Δd and Δk can be correctly predicted from the calculated ROS of the highest occupied σ molecular orbital.

The σ orbital ROS values are best understood with reference to the atomic orbital overlap integrals, which provide a quantitative measure of spatial orbital overlap for the four atomic orbitals involved in each case. The numerical values of the overlap integrals are included in Table 1 (middle) and plotted in Figures 1 and 2 as a function of bond distance from 0.8 to 2.0 Å. Plots such as these, for both σ and π MOs and over a much wider range of bond distances, have been published for N_2 and F_2[10a,18] and CO.[10b] The most noticeable feature of these plots is that the 2s−2s, $2p_\sigma$−2s, and 2s−$2p_\sigma$ spatial overlaps increase with decreasing bond distance, at least near the equilibrium bond distances. This is in contrast to the $2p_\sigma-2p_\sigma$ overlaps for all but F_2, which show a decrease with decreasing bond distance near the equilibrium bond distances. As pointed out previously[10b,18] this is due to an "overshooting the mark" phenomenon for these $2p_\sigma-2p_\sigma$ overlaps as the "front" lobe of one $2p_\sigma$ orbital begins to extend past the nucleus of the other atom to overlap in an antibonding way with the "rear" lobe of the other $2p_\sigma$ orbital, such that the optimal $2p_\sigma-2p_\sigma$ overlaps occur at distances about 0.5 Å longer than the equilibrium values. So, in contrast to π bonding interactions, increasingly favorable 2s−2s, $2p_\sigma$−2s, and 2s−$2p_\sigma$ spatial orbital overlaps are counterbalanced by unfavorable $2p_\sigma-2p_\sigma$ overlaps near the equilibrium bond distances for N_2, CO, BF, CN^-, and NO^+. Therefore the maximum $\sigma-\sigma$ net overlaps occur at distances only about 0.2 Å shorter than the equilibrium values for these molecules. The fact that equilibrium bond distances are in general somewhat longer than the optimum distances for orbital overlaps is due to Pauli (or "four-electron") repulsion between occupied atomic orbitals (or fragment molecular orbitals) on either side of the bond.[19]

Contour diagrams for the 4σ and 5σ MOs of N_2, CO, and BF at both the equilibrium and 2.0 Å distances are shown in

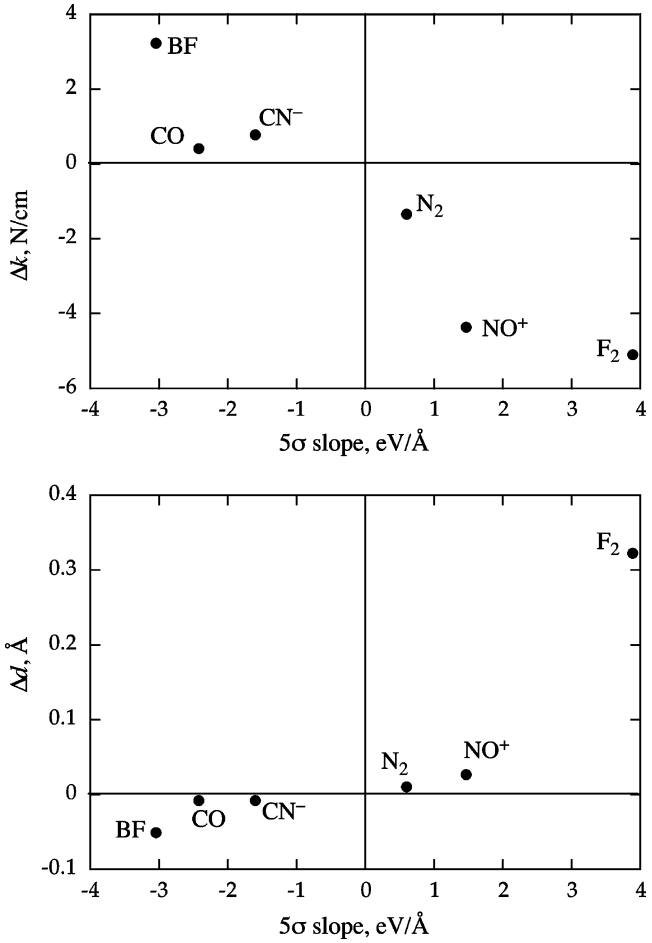

Figure 3. Plots of changes, upon 5σ 1-e$^-$ ionization, in calculated stretching force constants (Δk, top) and calculated equilibrium bond distances (Δd, bottom) as a function of the 5σ radial orbital energy slopes (ROSs; see Figure 1, middle) for F_2, N_2, CO, BF, CN^-, and NO^+.

Figure 4. The presence of a nodal plane for the 4σ orbital of N_2 is consistent with the weakly antibonding character and negative orbital energy slope for this orbital. Similarly, the lack of a nodal plane for the 5σ orbital of N_2 is consistent with its small positive slope at the equilibrium bond distance. In contrast to N_2, the 4σ orbital of BF lacks a node in the internuclear region, with the 4σ orbital energy slope (Table 1, middle) being of equal but opposite magnitude at the equilibrium distances for these molecules. As in the case of CO noted above, however, the 5σ orbital contour plots for both N_2 and BF do not contain a node in the internuclear region, even though N_2 has a small positive 5σ ROS and CO and BF both have small negative ROSs at the equilibrium distances (Table 1, middle). A given molecular orbital can exhibit any degree of bonding character, from strongly bonding through nonbonding to strongly antibonding. Although strongly bonding MOs may be characterized by the absence of an internuclear node and strongly antibonding orbitals by the presence of such a node, this is not the case for nonbonding, weakly bonding, and weakly antibonding orbitals, such as the 4σ and 5σ orbitals considered here.

Bonding in CO and the Nature of the 5σ MO. Frenking et al. claim that the observed bond contraction and increase in stretching force constant for CO^+ relative to CO occur as a result of an electrostatic effect.[10b] They did ADF calculations on CO with both H^+ and a unit point positive charge Q located on both the C and O ends of CO. We disagree with their claim that these calculations provide "a strong argument against an antibonding nature of the 7σ [5σ in our numbering scheme] HOMO of CO." The observed effects are a contraction of the C−O bond if H^+ is at the carbon side and an elongation if H^+

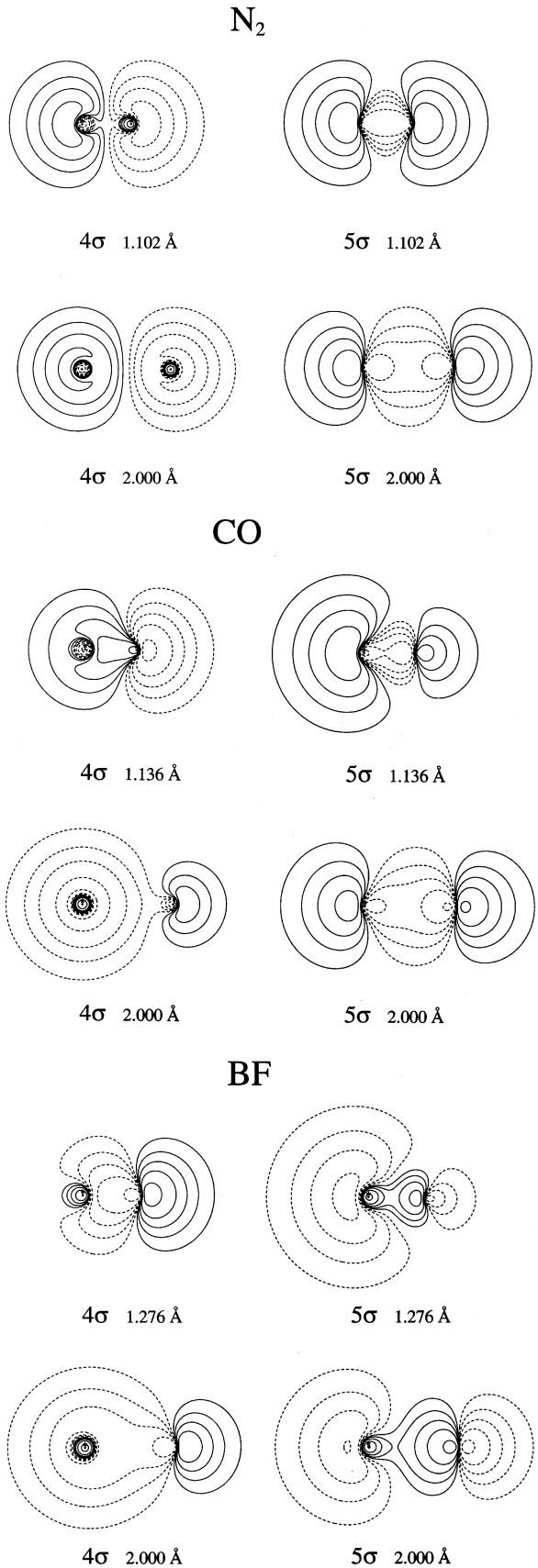

Figure 4. Contour plots of the 4σ and 5σ orbitals for N_2, CO, and BF at the calculated equilibrium distances (top figures) and at 2.0 Å (bottom figures).

is at the oxygen side. We also find these effects and have traced them to the somewhat better spatial overlap of the hydrogen 1s AO with the large carbon lobe and thus greater depopulation of the CO 5σ than 4 σ (0.84 e^- vs 0.04 e^-) if H^+ is at the C end, and the somewhat better overlap of the hydrogen 1s AO with the large oxygen lobe and thus greater depopulation of the CO 4σ than 5σ (0.50 e^- vs 0.15 e^-) if H^+ is at the O end (see Figure 4b). Frenking et al. argue that the nearly identical geometry changes for H^+, and with the orbital-free point charge Q, are evidence for an electrostatic effect. This argument is not valid. Apart from the evidence for orbital interaction effects that we mention above, a proton and point charge are physically and technically, *i.e.*, in the computations, identical. In particular, also in the absence of basis functions centered on Q, the function space of the latter is to a large extent described by the basis functions on C. This phenomenon is related to the basis set superposition error.

To avoid this problem, we did three electric field calculations for CO in which the positive end of a homogeneous electric field was oriented (i) along the molecular axis and toward the C end, (ii) along the molecular axis and toward the O end, and (iii) perpendicular to, and at the midpoint of, the molecular axis. Parenthetically we should stress that in principle another problem is associated with using homogeneous electric fields, namely, the loss of electrons through tunneling. This is not a significant factor in our calculations, however, because of the use of a basis set that is localized closely around the nuclei. For better comparison with Frenking's results for CO interacting with H^+ and Q, we have chosen the magnitude of the homogeneous electric field such that it corresponds to the magnitude of the radial electric field provided by a unit positive charge at a distance of 1 Å from C or O, respectively. Our calculations show that having the positive end of the electric field on the C side of CO effectively makes C more electronegative and O relatively less electronegative, thereby altering their relative 2s and $2p_z$ orbital energies such that C and O effectively "trade places" in the right side of Scheme 2, making the 4σ orbital localized on C and the 5σ orbital localized on O. Reversing the orientation of the electric field such that the positive end is on the O side of CO has the opposite effect, making the σ bonding situation for CO more like that for BF, *i.e.*, making 4σ even more O localized and 5σ even more C localized than in the absence of an electric field. Most importantly, such polarization or electrostatic effects are entirely consistent with the usual assumption that the 5σ HOMO of CO is slightly antibonding and localized on the C atom.

Interestingly, although the CO 5σ is definitely slightly antibonding at the equilibrium bond distance (*vide supra*), it does become slightly bonding at larger C−O distances. This can be seen in Figure 1, which shows that the 5σ ROS goes from slightly negative at C−O = 1.136 Å to slightly positive at larger C−O, *e.g.*, at 2 Å. This is easy to understand on the basis of the bonding mechanism discussed above. As the C−O bond stretches, the magnitude of all C−O overlap integrals decreases, with one exception: the $2p_\sigma$−$2p_\sigma$ overlap first increases and then, at longer distances, decreases more slowly than for the other overlap integrals. This is simply because the $2p_\sigma$ lobes that point toward and overlap each other at the equilibrium distance already penetrate into the backside lobes of the other $2p_\sigma$ AOs; this causes cancellation of overlap (*vide supra*). The consequence is that as the C−O bond elongates, the C 2s−O $2p_\sigma$ antibonding contribution to the CO 5σ fades out earlier than the C $2p_\sigma$ + O $2p_\sigma$ bonding contribution. This leads to the change from *slightly* antibonding to *slightly* bonding.

The relative increase of the C $2p_\sigma$ + O $2p_\sigma$ character in the 5σ orbital at longer CO distances is also nicely revealed by the contour plots in Figure 4b. At 1.135 Å, the CO 5σ orbital has a large amplitude on C consisting of carbon 2s and $2p_\sigma$ combined (*i.e.*, antibonding and bonding with O $2p_\sigma$, respectively; see Scheme 2) such that the resulting hybrid is pointing away from oxygen. Note that this leads to: (i) the large carbon lobe (which is important for the σ-donation capability of CO in coordination chemistry), and (ii) the shift of the C 2s−O $2p_\sigma$ "antibonding" nodal surface toward the carbon atom. *This* is why the amplitude of the 5σ orbital in between C and O is without a nodal surface; it stems mainly from one of the oxygen $2p_\sigma$ lobes. However, if the C−O bond is expanded to 2.0 Å, the C 2s−O $2p_\sigma$ antibonding component fades out of the 5σ orbital, which then acquires the appearance of the C $2p_\sigma$ + O $2p_\sigma$ orbital combination with an increased amplitude on the oxygen side (see Figure 4b).

Atomic Charge Distributions and Chemical Reactivities. We now consider the overall distribution of electric charge within the heteronuclear diatomic molecules considered here. VDD[9d−g] and Hirshfeld[14] atomic charges for these molecules are given in Table 1 (bottom) for 0.8 Å, equilibrium, and 2.0 Å bond distances. We focus our attention here on the uncharged CO and BF molecules because the variation in atomic charge with bond distance is greater than for the charged species NO^+ and CN^-. There is generally good agreement between the atomic charges calculated according to both the VDD and Hirshfeld definitions, the most notable feature being the steadily decreasing atomic charge on the less electronegative atom (C or B) as the bond distance decreases. In fact, the calculated VDD charges on both C and B actually reverse sign from positive to negative somewhere between the equilibrium bond distance and 0.8 Å for these two molecules such that both C and B bear negative charges. Note that 0.8 Å is an extremely short distance between two main group atoms. Not only is there excessive repulsion (see, *e.g.*, ref 18) but also the nucleus of one of the atoms, in a sense, begins to enter into the charge distribution of the other atom. In the present case, *i.e.*, with only moderately (at equilibrium distances) polarized diatomics, this causes the electropositive atom to become surrounded by electron density that at longer distances would be associated with the more electronegative atom. Consequently, the less electronegative atom can become effectively negatively charged at these exotically short bond distances. This explains the small (and in some cases even negative) VDD and Hirshfeld charges for the less electronegative atom (C in CO and B in BF) at 0.8 Å.

It is useful to compare calculated atomic charges for CO because values based on many other widely used definitions are available. As seen in Table 1, both the Hirshfeld and VDD definitions give a charge of about +0.08 on C at the equilibrium internuclear distance. The Mulliken charge calculated here of about +0.2 is very basis-set dependent, but a recent modification for calculating Mulliken charges that claims to reduce this limitation gives +0.061,[20] much closer to our VDD and Hirshfeld values. Other definitions that yield a similar charge include Cioslowski's atomic polar tensor method (+0.11),[21] Stone's distributed multipole analysis (+0.10),[6b] Roby-Cruickshank's (+0.07),[22] and Ehrhardt-Ahlrichs' (+0.06)[23] refinements of Davidson's projection-density method, and the simple electronegativity-equalized value of +0.17 (calculated by taking the electronegativity difference divided by its sum,[24] using Pauling-scale electronegativities of 2.57 and 3.65 for C and O, respectively[25]). As expected, NBO and AIM values of the atomic

charge (+0.48[26] and +1.22,[27] respectively) are significantly more positive than those of other commonly used definitions.[9,14c]

Regardless of the definition used, all values of the atomic charge on carbon cited here are positive. The negative end of the CO dipole moment points in the direction of the C atom, however.[28] This apparent paradox is well documented[28b,c] and is due to the large atomic dipoles on both C and O that both point in this direction (see Figure 4b), more than compensating for the transfer of molecular charge from C toward the more electronegative O atom.[26,28]

The negative atomic charge on the O atom in CO leads to preferential attack by protons at this side, in spite of the O atom being on the positive side of the CO dipole and in spite of HCO^+ being more thermodynamically stable than COH^+.[29] This charge effect is an example of Klopman's theorem for explaining hard acid-hard base interactions within the context of Pearson's hard and soft acid/base (HSAB) approach.[30] Klopman's theorem states that the preference of hard acids for hard bases is due to electrostatic effects (or "charge control"), so that the hard acid H^+ prefers to react with the hard, negatively charged O atom.[29a] In contrast, according to Klopman, reactions between soft Lewis acids and bases are best understood by frontier orbital overlap effects (or "orbital control"), which explains the well-known preference of metal atoms for the C atom when bonding to CO, the C atom being the "soft" end according to the HSAB approach. In fact, the Fukui functions for *both* nucleophilic and electrophilic attack of CO are substantially larger for C than O in CO,[31] the larger electrophilic value for C reflecting the more diffuse character of the 5σ HOMO localized on C compared to the less diffuse 4σ O-localized orbital (see Figure 4b). Similarly, the larger nucleophilic value for C, in apparent contradiction to the negative end of the CO dipole lying at the C end of the molecule, reflects the large amplitude of the 2π LUMO at this atom, and points to the importance of the shapes, sizes, and occupancies of frontier orbitals in governing the reactivity of a molecule.

Although CO normally functions as a net Lewis acid in its bonding to transition metals, with 5σ HOMO donation to the metal more than offset by 2π acceptance,[7,31b] the opposite is true for a class of more recently prepared carbonyl compounds,[7f,g,32] many of which bear a net positive charge. In these compounds there appears to be negligible acceptance of charge into the antibonding 2π LUMO, the metal−carbon bonds dominated instead by substantial 5σ donation of charge from CO to the metal atom. In these compounds the CO stretching force constant is greater than the value for free CO, an observation that can be explained by the nature of s−p σ orbital mixing in CO. As we demonstrated, such orbital mixing results in the 5σ HOMO being slightly antibonding, so that loss of electron density from this orbital, uncompensated by acceptance of charge into the antibonding 2π LUMO, accounts for the increase in the stretching force constant.

To understand these many-faceted properties of CO, it is essential to know relative atomic charges (the overall charge density distribution) and the bonding natures (bonding, nonbonding, or antibonding between C and O), energies, symmetries, shapes, and sizes of the frontier orbitals (and their resulting charge distribution). Of particular importance is the insight provided by knowing *which* frontier orbitals are responsible for a given bonding property; *i.e.*, CO is both a π-acid that accepts charge from metals through its 2π orbital localized on C and a σ-base that donates charge to metals through its 5σ orbital, also localized on C. High-level DFT calculations of the type now widely available with ADF and other programs readily provide all the requisite information. This allows deeper and more accurate insights into chemical reactivity and enriches our conceptual understanding of chemistry in general.

4. Conclusions

The present work confirms the value of the radial orbital-energy slope (ROS) criterion (*i.e.*, the slope of the orbital energy as a function of a bond length) as a general way of classifying individual molecular orbitals as bonding, nonbonding, or antibonding. High-level ADF calculations of Kohn−Sham orbital energies for second-period diatomic molecules allow us to establish a quantitative relationship between these ROS values and changes in stretching force constants and bond distances upon one-electron ionization of the highest occupied σ orbital (5σ in all cases). Negative ROS values, in which the orbital energy decreases with increasing internuclear distance, correspond to antibonding MOs, and lead to decreased bond distances and increased stretching force constants upon ionization. Conversely, orbitals with positive ROS values correspond to bonding MOs, and lead to increased bond distances and decreased stretching force constants upon ionization. The very small but negative 5σ ROS for CO and the very small but positive 5σ ROS for N_2 correspond to approximately nonbonding character for this orbital in both cases. However, the opposite signs of the ROSs for these molecules are consistent with the opposite effects of one-electron ionization on their bond strengths (as measured by stretching force constant changes) and lengths.

The claim that the 5σ HOMO of CO is bonding because of a lack of a nodal surface in the internuclear region for this orbital[10b] is demonstrated to be unreliable. At least for approximately nonbonding MOs, no such nodal surfaces are likely to be present, and the ROS criterion used here provides a quantitative and more reliable way of determining whether a given MO is bonding or antibonding. In fact, a given orbital can be weakly bonding at some bond distances and weakly antibonding at others, as is the case with the 5σ orbital of CO.

The ROS criterion for assigning MOs as bonding or antibonding is related to and complementary with the Walsh diagram interpretation of molecular bonding, which involves a consideration of orbital energy variations with changes in angular geometry. A thorough understanding of such frontier orbital properties, together with the charge distribution within a molecule, is possible with programs like ADF. As illustrated by Klopman's interpretation[30] of HSAB theory, such properties are necessary for a full appreciation of the chemical reactivity of any molecular species.

Acknowledgment. We thank The Netherlands Organization for Scientific Research (NWO-CW) for support of this work. J.K.N. thanks Bowdoin College for sabbatical leave support, including a Porter Fellowship.

Supporting Information Available: Figure showing molecular orbital correlation diagrams for N_2, CO, and BF, similar to those in Figure 1, but including both σ and π interactions. This material is available free of charge via the Internet at http://pubs.acs.org.

References and Notes

(1) For example: (a) Atkins, P.; Jones, L. *Chemical Principles*, 4th ed.; W. H. Freeman: New York, 2008; pp 115−128. (b) Brown, T. L.; LeMay, H. E., Jr.; Bursten, B. E.; Burdge, J. R. *Chemistry: The Central Science*, 9th ed.; Prentice Hall: Upper Saddle River, NJ, 2003; pp 343−355.

(2) (a) Haim, A. *J. Chem. Educ.* **1991**, *68*, 737−738. (b) Housecroft, C. E.; Constable, E. C. *Chemistry: An Integrated Approach*; Addison Wesley Longman: Harlow, England, 1997; pp 135−137. (c) Winter, M. J.

Chemical Bonding; Oxford: New York 1996; pp 47−49. (d) Allan, M. *J. Chem. Educ.* **1987**, *64*, 418−424. (e) DeKock, R. L.; Gray, H. B. *Chemical Structure and Bonding*; University Science Books: Mill Valley, CA, 1989; pp 223−228.

(3) (a) Housecroft, C. E.; Sharpe, A G. *Inorganic Chemistry*; Pearson Education: Harlow, England, 2005; pp 41−43 (b) Reference 2b, pp 176−183. (c). Reference 2c, pp 53−56. (d) Reference 2e, pp 255−260.

(4) Ziegler, T. *Chem. Rev.* **1991**, *91*, 651−667.

(5) (a) Bickelhaupt, F. M.; Baerends, E. J. In *Reviews in Computational Chemistry*; Lipkowitz, K. B., Boyd, D. B., Eds.; Wiley-VCH: New York, 2000; Vol. 15, pp 1−86. (b) Velde, G. te; Bickelhaupt, F. M.; Baerends, E. J.; van Gisbergen, S. J. A.; Fonseca Guerra, C.; Snijders, J. G.; Ziegler, T. *J. Comput. Chem.* **2001**, *22*, 931−967.

(6) (a) He, Y.; Gräfenstein, J.; Kraka, E.; Cremer, D. *Mol. Phys.* **2000**, *98*, 1639−1658. (b) Cohen, A. J.; Tantirungrotechai, Y. *Chem. Phys. Lett.* **1999**, *299*, 465−472.

(7) (a) Diefenbach, A.; Bickelhaupt, F. M.; Frenking, G. *J. Am. Chem. Soc.* **2000**, *122*, 6449−6458. (b) Radius, U.; Bickelhaupt, F. M.; Ehlers, A. W.; Goldberg, N.; Hoffmann, R. *Inorg. Chem.* **1998**, *37*, 1080−1090. (c) Ehlers, A. W.; Baerends, E. J.; Bickelhaupt, F. M.; Radius, U. *Chem. Eur. J.* **1998**, *4*, 210−221. (d) Pearson, R. G. *Inorg. Chem.* **1984**, *23*, 4675−4679. (e) Elschenbroich, C. *Organometallics*, 3rd ed.; Wiley-VCH: Weinheim, 2006; pp 363−372. (f) Strauss, S. H. *J. Chem. Soc., Dalton Trans.* **2000**, 1−6. (g) Willner, H.; Aubke, F. *Angew. Chem.* **1997**, *209*, 2505−2530; Angew. *Chem., Int. Ed. Engl.* **1997**, *36*, 2403−2425.

(8) (a) Herzberg, G. *Molecular Spectroscopy and Molecular Structure, Vol. 1: Diatomic Molecules*; Prentice Hall: New York, 1939; p 388. (b) Herzberg, G. *Molecular Spectra and Molecular Structure, Vol. 1: Spectra of Diatomic Molecules*; van Nostrand: New York, 1950; pp 362−363. (c) Woodward, R. B.; Hoffmann, R. *The Conservation of Orbital Symmetry*; Verlag Chemie: Weinheim, 1971; p 18. (d) Lee, H. Y.; Wang, S. P.; Chang, T. C. *Int. J. Quantum Chem.* **2001**, *81*, 53−65.

(9) (a) Jug, K.; Maksic, Z. B. The Meaning and Distribution of Atomic Charges in Molecules. In *Molecular Spectroscopy, Electronic Structure and Intramolecular Interactions*; Maksic, Z. B., Ed.; Springer-Verlag: Berlin, 1991; pp 236−288. (b) Wiberg, K. B. *J. Chem. Educ.* **1996**, *73*, 1089−1095. (c) Wiberg, K. B.; Rablen, P R. *J. Comput. Chem.* **1993**, *14*, 1504−1518. (d) Bickelhaupt, F. M.; van Eikema Hommes, N. J. R.; Fonseca Guerra, C.; Baerends, E. J. *Organometallics* **1996**, *15*, 2923−2931. (e) Fonseca Guerra, C.; Bickelhaupt, F. M.; Snijders, J. G.; Baerends, E. J. *Chem. Eur. J.* **1999**, *5*, 3581−3594. (f) Fonseca Guerra, C.; Handgraaf, J. W.; Baerends, E. J.; Bickelhaupt, F. M. *J. Comput. Chem.* **2004**, *25*, 189−210. Voronoi cells are equivalent to Wigner-Seitz cells in crystals; for the latter, see: (g) Kittel, C. *Introduction to Solid State Physics*; Wiley: New York, 1986.

(10) (a) Esterhuysen, C.; Frenking, G. *Theor. Chem. Acc.* **2004**, *111*, 381−389. (b) Frenking, G.; Loschen, C.; Krapp, A.; Fau, F.; Strauss, S. H. *J. Comput. Chem.* **2007**, *28*, 117−126.

(11) (a) Fonseca Guerra, C.; Snijders, J. G.; te Velde, G.; Baerends, E. J. *Theor. Chem. Acc.* **1998**, *99*, 391−403. (b) Fonseca Guerra, C.; Visser, O.; Snijders, J. G.; te Velde, G.; Baerends, E. J. In *Methods and Techniques for Computational Chemistry*; Clementi, E., Corongiu, G., Eds.; STEF: Cagliari, 1995; pp 305−395. (c) Baerends, E. J.; Ellis, D. E.; Ros, P. *Chem. Phys.* **1973**, *2*, 41−51. (d) Boerrigter, P. M.; te Velde, G.; Baerends, E. J. *Int. J. Quantum Chem.* **1988**, *33*, 87−113. (e) te Velde, G.; Baerends, E. J. *J. Comput. Phys.* **1992**, *99*, 84−98. (f) Snijders, J. G.; Baerends, E. J.; Vernooijs, P. *At. Nucl. Data Tables* **1981**, *26*, 483−509. (g) Krijn, J.; Baerends, E. J. *Fit Functions in the HFS Method; Internal Report* (in Dutch); Vrije Universiteit: Amsterdam, 1984. (h) Slater, J. C. *Quantum Theory of Molecules and Solids Vol. 4*; McGraw-Hill: New York, 1974. (i) Vosko, S. H.; Wilk, L.; Nusair, M. *Can. J. Phys.* **1980**, *58*, 1200−1211. (j) Becke, A. D. *J. Chem. Phys.* **1986**, *84*, 4524−4529. (k) Becke, A. *Phys. Rev. A* **1988**, *38*, 3098−3100. (l) Perdew, J. P. *Phys. Rev. B* **1986**, *33*, 8822−8824; Erratum. *Phys. Rev. B* **1986**, *34*, 7406. (m) Fan, L.; Ziegler, T. *J. Chem. Phys.* **1991**, *94*, 6057−6063. (n) Schipper, P. R. T.; Gritsenko, O. V.; van Gisbergen, S. J. A.; Baerends, E. J. *J. Chem. Phys.* **2000**, *112*, 1344−1352.

(12) (a) Chang, C.; Pelissier, M.; Durand, P. *Phys. Scr.* **1986**, *34*, 394−404. (b) van Lenthe, E.; Baerends, E. J.; Snijders, J. G. *J. Chem. Phys.* **1973**, *99*, 4597−4610. (c) van Lenthe, E.; van Leeuwen, R.; Baerends, E. J.; Snijders, J. G. *Int. J. Quantum Chem.* **1996**, *57*, 281−293.

(13) (a) Hamil, S.; Duffy, P.; Casida, M. E.; Salahub, D. R. *J. Electron Spectrosc. Relat. Phenom.* **2002**, *123*, 345−363. (b) Chong, D. P.; Gritsenko, O. V.; Baerends, E. J. *J. Chem. Phys.* **2002**, *116*, 1760−1772.

(14) (a) Hirshfeld, F. L. *Theor. Chim. Acta* **1977**, *44*, 129−138. For recent critical perspectives on this definition see: (b) Parr, R. G.; Ayers, P. W.; Nalewajski, R. F. *J. Phys. Chem. A* **2005**, 3957−3959. (c) Bultinck, P.; Van Alsenoy, C.; Ayers, P. W.; Carbó-Dorca, R. *J. Chem. Phys.* **2007**, *126*, 144111 (1−9). (d) Mandado, M.; Van Alsenoy, D.; Mosquera, R. A. *J. Phys. Chem. A* **2004**, *108*, 7050−7055.

(15) (a) Huber, K. P.; and Herzberg, G. *Molecular Spectra and Molecular Structure IV. Constants of Diatomic Molecules*; Van Nostrand Reinhold: New York, 1979. (b) Khristenko, S. V.; Maslov, A. I.; Shevelko, V. P. *Molecules and Their Spectroscopic Properties*; Springer: Heidelberg, 1998. (c) Nakamoto, K. *Infrared and Raman Spectra of Inorganic and Coordination Compounds*, 5th ed.; Wiley: New York, 1997.

(16) (a) Hawthorne, M. F.; Wegner, P. A.; Stafford, R. C. *Inorg. Chem.* **1965**, *4*, 1673−1675. (b) Graham, W. A. G. *Inorg. Chem.* **1968**, *7*, 315−321. (c) Hall, M. B.; Fenske, R. F. *Inorg. Chem.* **1972**, *11*, 768−775.

(17) ROS values (eV/Å) computed at BP86 with various basis sets for the CO 4σ and 5σ MOs, respectively: +0.54, +0.67 (SZ), −1.54, −2.58 (DZ), −1.00, −2.79 (DZP), −0.53, −2.44 (TZP), −0.57, −2.44 (TZ2P), −0.45, −2.33 (QZ4P).

(18) Krapp, A.; Bickelhaupt, F. M.; Frenking, G. *Chem. Eur. J.* **2006**, *12*, 9196−9216.

(19) See, for example: (a) Bickelhaupt, F. M.; DeKock, R. L.; Baerends, E. J. *J. Am. Chem. Soc.* **2002**, *124*, 1500. (b) Bickelhaupt, F. M.; Baerends, E. J. *Angew. Chem.* **2003**, *115*, 4315; *Angew. Chem., Int. Ed.* **2003**, *42*, 4183. (c) Ref. 5a

(20) (a) Sato, H.; Sakaki, S. *Chem. Phys. Lett.* **2007**, *434*, 165−169. (b) See also the Modified Mulliken approach proposed in Ref. 9d.

(21) Cioslowski, J. *J. Amer. Chem. Soc.* **1989**, *111*, 8333−8336.

(22) Cruickshank, D. W. J.; Avramides, E. J. *Philos. Trans. R. Soc. London, Ser. A* **1982**, *304*, 533−565.

(23) Ehrhardt, C.; Ahlrichs, R. *Theor. Chim. Acta* **1985**, *68*, 231−245.

(24) Bratsch, S. G. *J. Chem. Educ.* **1984**, *61*, 588−589. More elaborate ways of calculating electronegativity-equalized charges are available: Gutiérrez-Olivia, S.; Jaque, P.; Toro-Labbé, A. *J. Phys. Chem. A* **2000**, *104*, 8955−8964.

(25) Nagle, J. K. *J. Am. Chem. Soc.* **1990**, *112*, 4741−4747.

(26) He, Y.; Gräfenstein, J.; Kraka, E.; Cremer, D. *Mol. Phys.* **2000**, *98*, 1639−1658.

(27) (a) Cortés-Guzmán, F.; Bader, R. F. W. *Coord. Chem. Rev.* **2005**, *249*, 633−662. (b) Bader, R. F. W.; Matta, C. F. *J. Phys. Chem. A* **2004**, *108*, 8385−8394.

(28) (a) Muenter, J. S. *J. Mol. Spectrosc.* **1975**, *55*, 490−491. (b) Laidig, K. E. *Can. J. Chem.* **1996**, *74*, 1131−1138. (c) Gillespie, R. J.; Popelier, P. L. A. *Chemical Bonding and Molecular Geometry*; Oxford University Press: New York, 2001; pp 43−47, 208−209.

(29) (a) Chattaraj, P. K.; Maiti, B. *J. Am. Chem. Soc.* **2003**, *125*, 2705−2710. (b) Rosati, R. E.; Skrzypkowski, M. P.; Johnsen, R.; Golde, M. F. *J. Chem. Phys.* **2007**, *126*, 154302 (1−8). (c) Gudean, C. S.; Woods, R. C. *Phys. Rev. Lett.* **1982**, *48*, 1344−1348. (d) Woods, R. C.; Gudeman, C. S.; Dickman, R. L.; Goldsmith, P. F.; Huguenin, G. R.; Irvine, W. M.; Hjalmarson, A.; Nyman, L. A.; Olofsson, H. *Astrophys. J.* **1983**, *270*, 583−588.

(30) Klopman, G. *J. Am. Chem. Soc.* **1968**, *90*, 223−234. For modern DFT perspectives on charge versus orbital control of acid-base reactions see: Anderson, J. S. M.; Melin, J.; Ayers, P. W. *J. Chem. Theory Comput.* **2007**, *3*, 358−374; 375−389 and Ayers, P. W. *J. Chem. Phys.* **2005**, *122*, 141102 (1−3).

(31) (a) Sablon, N.; De Proft, F.; Ayers, P. W.; Geerlings, P. *J. Chem. Phys.* **2007**, *126*, 224108 (1−6). (b) Lee, C.; Yang, W.; Parr, R. G. *J. Molec. Struct. (THEOCHEM)* **1988**, *163*, 305−313.

(32) (a) Lupinetti, A. J.; Fau, S.; Frenking, G.; Strauss, S. H. *J. Phys. Chem. A* **1997**, *101*, 9551−9559. (b) Aubke, F.; Wang, C. *Coord. Chem. Rev.* **1994**, *137*, 483−524.